Thermal exchange radius measurement: Application to nanowire thermal imaging

Cite as: Rev. Sci. Instrum. **81**, 073701 (2010); https://doi.org/10.1063/1.3455214
Submitted: 26 March 2010 . Accepted: 25 May 2010 . Published Online: 02 July 2010

Etienne Puyoo, Stéphane Grauby, Jean-Michel Rampnoux, Emmanuelle Rouvière, and Stefan Dilhaire

Thermal exchange radius measurement: Application to nanowire thermal imaging

Etienne Puyoo,[1,2] Stéphane Grauby,[1,a)] Jean-Michel Rampnoux,[1] Emmanuelle Rouvière,[2] and Stefan Dilhaire[1]
[1]*CPMOH, Université Bordeaux 1, 351, Cours de la Libération, 33405 Talence Cedex, France*
[2]*CEA - DRT/LITEN/DTNM, LCRE, 17 Rue des Martyrs, 38 054 Grenoble Cedex, France*

(Received 26 March 2010; accepted 25 May 2010; published online 2 July 2010)

In scanning thermal microscopy (SThM) techniques, the thermal exchange radius between tip and sample is a crucial parameter. Indeed, it limits the lateral spatial resolution but, in addition, an accurate value of this parameter is necessary for a precise identification of thermal properties. But until now, the thermal exchange radius is usually estimated but not measured. This paper presents an experimental procedure, based on the 3ω-SThM method, to measure its value. We apply this procedure to evaluate the thermal exchange radius of two commercial probes: the well-known Wollaston one and a new probe constituted of a palladium film on a SiO_2 substrate. Finally, presenting silicon nanowire images, we clearly demonstrate that this new probe can reach a spatial resolution better than 100 nm whereas the Wollaston probe hardly reaches a submicronic spatial resolution. © *2010 American Institute of Physics.* [doi:10.1063/1.3455214]

I. INTRODUCTION

In recent years, the thermal characterization of devices and materials at submicrometric scales has become a major issue regarding advances in nanotechnology and material science. Hence, there is a need of techniques able to reach a nanometric lateral spatial resolution. Optical methods such as infrared thermometry,[1,2] visible thermoreflectance,[3–5] or interferometry,[5,6] which are diffraction limited, cannot reach such a resolution. Since its invention in 1986, the scanning thermal microscopy (SThM)[7] is presented as the most efficient technique to study thermal transport in nano-objects and nanomaterials. It is based on an atomic force microscope equipped with a thermal probe to carry out thermal images while simultaneously obtaining contact mode topography images.[7–9] The SThM has two different working configurations: the active and the passive modes. In the passive mode, the sample is locally heated and the passive probe, used as a thermometer, generates a thermal map. In 2000, Shi *et al.*[10,11] thus sensed the temperature distribution in current-carrying carbon nanotubes with a spatial resolution around 50 nm. On the contrary, in the active mode, the tip also serves as a heater. By measuring the tip temperature, we can evaluate the tip-to-sample heat flux exchange, which depends, among other things, on the sample thermal properties. Then, the SThM in active mode can sense local thermal properties.[12,13] In 2008, using this mode, Hinz *et al.*[14] determined the thermal conductivity of a 3 nm thick HfO_2 film with a spatial resolution around 25 nm. Nevertheless, the probe plays a crucial role to achieve nanothermal analysis with SThM and these low spatial resolutions are not obtained with commercial probes but with home-made probes, which represent a technological difficulty. With commercial probes, such as the classical well-known Wollaston one, which is the most commonly used probe, the resolution is of the order of 1 μm and hardly lower.[15]

Anyway, whether it is with home-made or with commercial probes, the spatial resolution limitation is dependent on the thermal exchange radius r_{th} between tip and sample.[16] Moreover, thermal conductivity measurements performed with SThM are correlated with this parameter r_{th}.[16,17] Hitherto in literature, r_{th} is either taken equal to the solid tip-apex radius evaluated from scanning electron microscopy (SEM) pictures[14] or evaluated as an adjustable parameter in a thermal model.[16,17] Actually, r_{th} is strongly dependent on the tip sharpness and the environmental conditions. Under atmospheric conditions, the two dominant tip-to-sample heat transfer mechanisms are conducted through a water meniscus bridging the tip and sample, and through the surrounding air. The solid-solid conduction through the contact is indeed not the main heat transfer. However, even for a same probe under the same experimental conditions, r_{th} estimation is very dependent on the model: around 200 nm in[17] but 2.32 μm in[16], in both cases for a Wollaston probe under the same environmental conditions, thus more than a one order of magnitude difference. Therefore, there is a need to precisely determine r_{th} and according to the authors' knowledge, there is no experiment to measure it accurately.

To measure r_{th}, we propose a simple experiment for which the tip is used in the active SThM working configuration performed in the ac-regime using the 3ω-method.[17] Hence, Sec. II recalls the principle of the 3ω-method. Then, Sec. III describes the two commercial probes for which we have tested the r_{th} measurement procedure: the classical Wollaston one and a new commercial Pd/SiO_2 probe (from Anasys Instruments). We present a geometrical description but, for each probe, we also measure its cut-off frequency which determines the experimental conditions such as the working

a)Electronic mail: stephane.grauby@u-bordeaux1.fr.

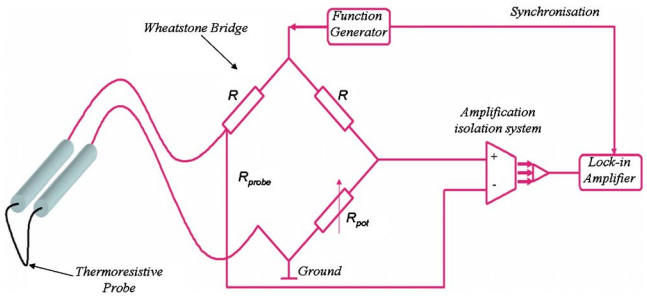

FIG. 1. (Color online) 3ω-SThM principle.

frequency and acquisition speed used in Sec. IV. In this last section, we explain the r_{th} measurement experimental procedure based on the 3ω-method described in Sec. II and under the experimental conditions determined in Sec. III. We measure the thermal exchange radius for both probes and we show, in particular, that the Pd/SiO_2 probe has a thermal exchange radius much smaller than the classical Wollaston probe. Finally, silicon nanowire topographic and 3ω thermal images obtained with both probes underline the influence of the thermal exchange radius on the spatial resolution.

II. 3ω-STHM PRINCIPLE

The r_{th} measurement procedure is based on an active 3ω detection method whose principle we first recall (Fig. 1). Whatever the probe, it is included in a Wheatstone bridge connected to an amplification isolation system. The variable resistor R_{pot} is adjusted so that its electrical resistance should be equal to the probe electrical resistance. A lock-in measurement of the amplification isolation system output voltage enables the SThM setup to work in a 3ω detection configuration: the function generator provides an ω electrical excitation pulsation voltage and hence an ω pulsation alternative current passes through the probe which warms up due to Joule effect. The dissipated heat flux P_{Joule} in the probe can be written as

$$P_{Joule} = R(T)\frac{I_0^2}{2}[1 + \cos(2\omega t)], \tag{1}$$

where $R(T)$ is the temperature dependent electrical resistance of the probe and I_0 is the alternative current amplitude. Consequently, the tip temperature variations ΔT_{tip} can be related to the static temperature variation amplitude T_{dc} and the second harmonic temperature variation one $T_{2\omega}$,

$$\Delta T_{tip} = T_{dc} + T_{2\omega}\cos(2\omega t + \phi), \tag{2}$$

where ϕ is the phase difference between the thermal and electrical signals. The 3ω tip voltage $V_{3\omega}$ is then expressed as follows:

$$V_{3\omega} = \frac{R_0 \alpha I_0 T_{2\omega}}{2}\cos(3\omega t + \phi), \tag{3}$$

where α is the probe temperature coefficient in K^{-1} and R_0 is the probe electrical resistance at room temperature in Ω. A lock-in measurement of $V_{3\omega}$ leads to the $T_{2\omega}$ probe temperature variations at 2ω, which depend on the probe environment. The more conductive the sample, the lower the 2ω thermal variations. More precisely, the $T_{2\omega}$ tip temperature variations depend on an equivalent thermal conductance G_{eq} which is the connection of the tip-to-sample contact thermal conductance G_C and of the sample thermal conductance G_S,

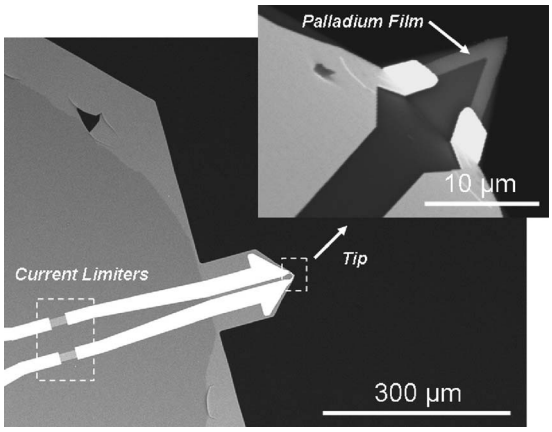

FIG. 2. SEM pictures of the Pd/SiO_2 probe.

$$\frac{1}{G_{eq}} = \frac{1}{G_C} + \frac{1}{G_S}. \tag{4}$$

G_C depends on the thermal exchange surface, hence on the tip-to-sample thermal exchange radius r_{th}, and G_S depends on the sample thermal conductivity λ_S and on r_{th}.[16–19] Obviously, to determine the sample thermal conductance and hence its thermal conductivity, it is necessary to develop a thermal model that describes the probe thermal behavior.[17] Based on Eq. (4), most of the models describing the thermal contact use two parameters in order to deduce λ_S: the contact thermal conductance G_C and the thermal contact radius r_{th}. Therefore, as r_{th} not only limits the spatial resolution but also constitutes a crucial parameter of the model describing the tip-to-sample thermal exchange, an essential preliminary step consists of evaluating r_{th}. Consequently, we will present in Sec. IV an experimental procedure, based on the active 3ω method described above, to measure it. This measurement method will be applied to two commercial probes we present in Sec. III.

III. PROBES GEOMETRICAL AND ELECTRICAL CHARACTERISTICS

The first probe is a "V" shape Wollaston tip[13,17] made of a 5 μm diameter platinum rhodium core covered with a 250 μm diameter silver coating which has been suppressed at the tip apex over a 200 μm length. The uncovered platinum core plays the role of the thermoresistive element. Its electrical resistance at room temperature is $R_0 = 2.5\ \Omega$ and its temperature coefficient is $\alpha = 1.65 \times 10^{-3}\ K^{-1}$.

The second probe is a new commercial Pd/SiO_2 probe (from Anasys Instruments). Figure 2 shows SEM pictures of this probe. It is a specially designed SiO_2 silica contact mode probe that incorporates a thin palladium (Pd) film near the apex of the tip. Two nickel chromium current limiters are placed upstream from the tip. Here, the thin Pd film acts as the thermoresistive element. Its electrical resistance at room temperature is $R_0 = 400\ \Omega$ and its temperature coefficient is

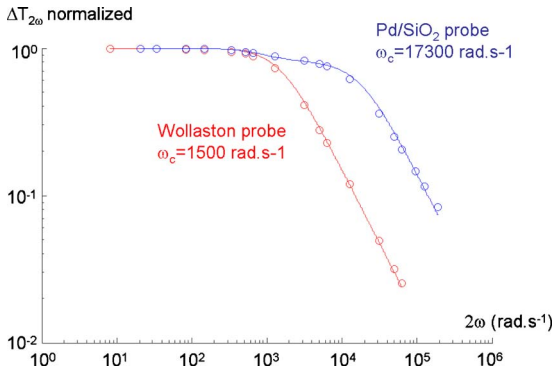

FIG. 3. (Color online) Normalized modulus of the 2ω temperature variations of the two different probes out of contact.

$\alpha = 1.2 \times 10^{-3}$ K^{-1}. For both probes, the current I_0 is chosen so that the amplitude of the dissipated heat flux in the probe as described in Eq. (1) should be of the order of 500 μW.

Now, it is useful to determine the probe cut-off frequency in order to choose the appropriate ω experimental pulsation of the function generator. Indeed, the probe behaves as a low-pass filter.[20] So, if we do not want to attenuate the thermal signal, we must choose a working frequency within the probe bandwidth. But, in addition, the probe cut-off frequency or its thermal time response rules the maximum scan speed achievable to carry out thermal imaging. Indeed, the time spent on each measurement point must be several times higher than the lock-in time constant, which in turn must be several times higher than the thermal excitation period of the signal. Consequently, the cut-off frequency limits the acquisition speed. Practically, choosing the time spent on each point at least ten times higher than the thermal period is a good compromise to keep a fast acquisition speed without affecting the 3ω signal.

Therefore, we measured the Bode response of both probes (Fig. 3), collecting the $V_{3\omega}$ amplitude, hence the temperature variation $T_{2\omega}$, as a function of the thermal pulsation 2ω. We clearly note that the $2f$ thermal cut-off frequency of the Pd/SiO_2 probe (2750 Hz) is 11.5 times higher than the Wollaston one (240 Hz). The acquisition time is then reduced by the same factor.

In the experiments described in Sec. IV, we will then choose a $f = 100$ Hz electrical excitation frequency for the Wollaston probe and $f = 1$ kHz for the Pd/SiO_2 probe. Hence, the thermal excitation frequencies are respectively 200 Hz and 2 kHz. Then the measurement time spent on each point is 50 ms for the Wollaston probe and 5 ms for the Pd/SiO_2 one. Typically, for a 256×256 point image, we reduce the image acquisition time from about 1 h with a Wollaston probe to less than 6 min with a Pd/SiO_2 probe.

IV. THERMAL EXCHANGE RADIUS MEASUREMENT AND NANOWIRE TOPOGRAPHIC AND THERMAL IMAGES

The experimental procedure consists of applying the 3ω method scanning the probe on an abrupt step. In our case, the step is made of a 200 nm thick oxide layer on a Si substrate. The sample is a commercial one. It has been fabricated using a highly anisotropic dry etch process. The incertitude on the 200 nm step height is ± 4 nm. Figure 4(a) presents the topographic (height curves) and thermal profiles ($T_{2\omega}$ curves) obtained with both probes along a 4 μm scan. For both height

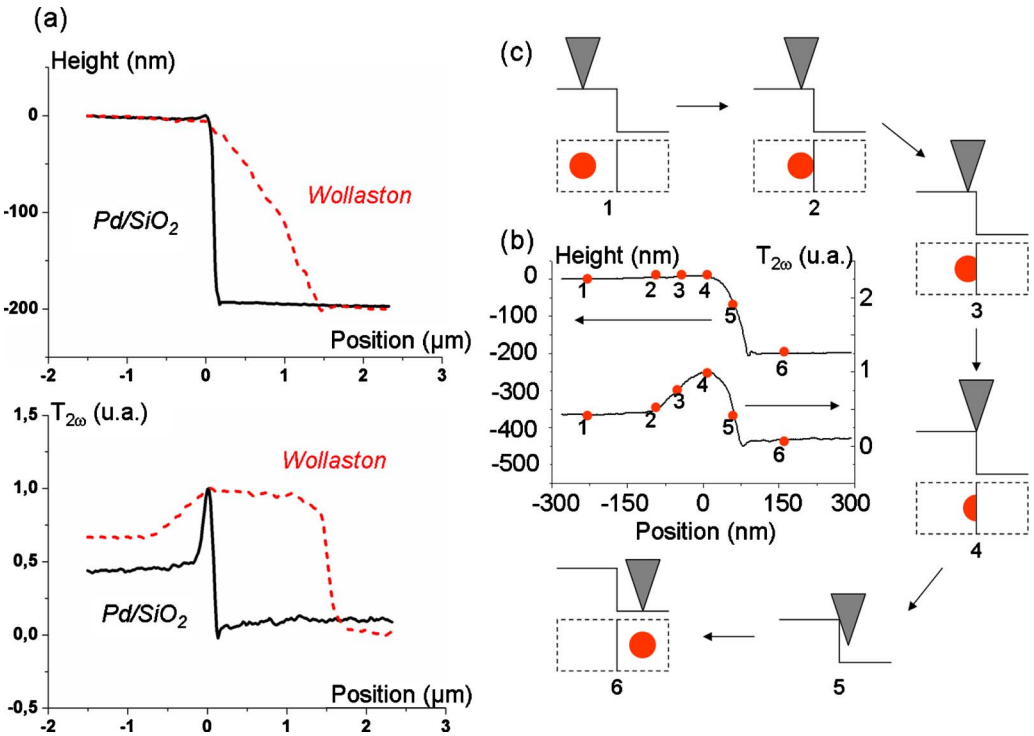

FIG. 4. (Color online) Topographic and thermal profiles obtained with the two different probes scanning an abrupt oxide on silicon step: (a) comparison of the profiles: the dotted line and the full line correspond to the profiles obtained respectively with the Wollaston and the Pd/SiO_2 probes. (b) Zoom on profiles obtained with the Pd/SiO2 probe. (c) Schematic side view of the probe and schematic top view of the thermal exchange surface.

and thermal signals, the Wollaston curves show a slow transition between the oxide step and the Si substrate. The transition is much more abrupt with the Pd/SiO_2 probe.

Figure 4(b) is a zoom of both signals obtained with the Pd/SiO_2 tip. Each red point corresponds to a position of the tip as represented in Fig. 4(c). In position 1, the tip is placed upon the oxide layer on top of the abrupt step. The gray triangle is a side schematic view of the apex of the tip scanning the sample, and the red disk is a top representative view of the thermal exchange surface. Then (position 2), the probe is shifted to the right toward the step. The height and thermal profiles remain constant. In position 3, the exchange surface is truncated because of the nearby abrupt step. The contact thermal resistance is indeed increased and the tip temperature increases. In position 4, the contact point is on the edge of the step. The contact thermal resistance rises and the tip temperature is maximal. Between positions 2 and 4, the thermal signal increase is probably also due to a thermal constriction modification. Nevertheless, we can consider that the spreading of the flux lines in the sample is confined in a semisphere with a radius equal to r_{th}. Therefore, we can assume that the difference between positions 4 and 2 corresponds to r_{th}. At stage 5, the probe is stepping off and the thermal contact point is done from the tip side. The thermal signal is not really useful but, on the topographic profile obtained with the Wollaston tip in Fig. 4(a), we have previously noted a slow transition between the oxide step and the Si substrate indicative of an important effect of the tip-sample geometry convolution. Finally (stage 6), the tip scans the Si substrate. The thermal and topographic profiles remain constant. The thermal signal at stage 6 is lower than at stage 1 because the Si thermal conductivity is higher than the oxide one.

Then, from Fig. 4(b), we have measured $r_{th}=100$ nm for the Pd/SiO_2 probe. We have repeated the measurement on different places along the step with the same probe and no significant dispersion has been observed on the evaluated r_{th}. As for the Wollaston probe, we have measured $r_{th}=820$ nm. Let us underline that, despite a classical value around 1 μm,[21,22] in agreement with the value we have measured, the estimated r_{th} from models for the Wollaston tip presents a wide disparity with values varying from 200 nm[17] to 2.32 μm,[16] hence the necessity to measure it experimentally since we recall that thermal conductivity measurements in the active mode are correlated with r_{th}. Depending on the sample geometry, the sample conductance G_s, to which the SThM in active mode is sensitive, is proportional to r_{th}[17] or to r_{th}^2.[14] For example, in the precise case of a semi-infinite layer, G_s is defined by the constriction of the thermal flux lines. According to Maxwell,[19] the thermal constriction conductance is

$$G_S = 4\lambda_S r_{th}, \tag{5}$$

where λ_S is the sample thermal conductivity. Thus, if r_{th} is estimated twice higher than its real value, it leads to a λ_S twice lower than its real value.

In addition, the lower value of r_{th} will lead to a better spatial resolution in thermal images. Indeed, when doing topographic images in contact mode, the spatial resolution is limited by the tip geometry since the topographic image is

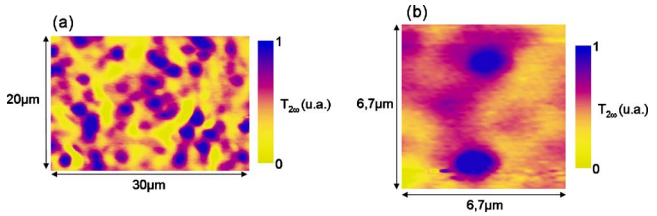

FIG. 5. (Color online) SThM imaging of silicon nanowires embedded in a silica matrix: (a) 20×30 μm^2 thermal image and (b) 6.7×6.7 μm^2 thermal image obtained with the Wollaston probe.

the convolution of the sample topography with the tip geometry, as previously noted in Fig. 4(a). But when doing 3ω thermal images, the spatial resolution is then also limited by the tip-sample thermal exchange surface.

Then, using both probes, we have made topographic and thermal images of silicon nanowires. The sample is an assembly of Si nanowires embedded in a silica SiO_2 die. Their diameters vary from 30 to 80 nm with a 50 nm mean value. Many nanowires jut out above the silica die of a few tens of nanometers. The Si nanowires have been grown via Au catalyzed vapor liquid solid reaction in an epitaxial chamber.[23] The nanowires are first oxide etched with a HF solution and the Au catalyzer residues are suppressed with a $IK:I_2$ solution. The nanowire array is then encapsulated by spin-coating a solution of spin-on glass material on the substrate. The sample top surface is then submitted to a chemical mechanical polishing process in order to reduce surface roughness and, hence, to facilitate the SThM scanning. A final etch is realized with a HF solution during a few seconds to ensure a good digging out of the nanowires.

Figure 5 presents two 3ω thermal images obtained with the Wollaston probe: Fig. 5(a) is a 20×30 μm^2 large image and Fig. 5(b) is a 6.7×6.7 μm^2 small image. We can detect a thermal contrast indicative of the presence of the nanowires. We have evaluated their diameter, measuring the full width at half maximum on the 3ω thermal signal. The smallest diameter we have measured is then 865 nm and the mean diameter measured on several nanowires is 1.27 μm. We hence confirm that the Wollaston spatial resolution is hardly submicrometric.[12,16] That means that we probably detect a collection of nanowires but certainly not individual nanowires. Moreover, usually, when doing thermal image using a Wollaston probe, the first step consists of doing a topographic image with a classical topographic probe to have a submicrometric resolution and localize the nanowires. Then, the probe is changed and a thermal image is made with the Wollaston probe. It is hence a long procedure and it is quasi impossible to image the same part of the sample and hence to correlate and interpret both images.

On the contrary, with the Pd/SiO_2 probe, we detect individual nanowires in both topographic [Fig. 6(a)] and 3ω thermal images [Fig. 6(b)] which are simultaneously obtained. In Fig. 6(b), the measured mean diameter of the nanowires, always estimated by the full width at half maximum on several nanowires, is 91 nm. The smallest measured diameter is 78 nm. Therefore, the Wollaston probe can only lead to measure the thermal properties of a nanowire collection whereas the Pd/SiO_2 tip can lead to thermal properties

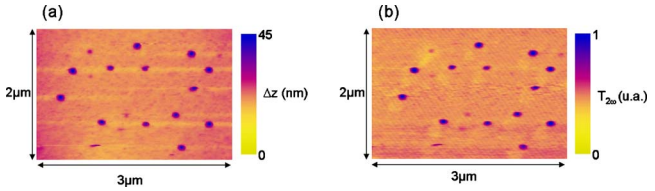

FIG. 6. (Color online) SThM imaging of silicon nanowires embedded in a silica matrix: (a) topographic image and (b) thermal image obtained with the Pd/SiO_2 probe.

of a single nanowire. As expected from the thermal exchange radius measurement, the spatial resolution is far better with the Pd/SiO_2 probe which has the smallest thermal exchange radius. This spatial resolution has already been obtained for thermal imaging but using home-made probes,[10,11,14] which imply heavy chemical equipment, and not using commercial probes.

V. CONCLUSIONS

We have proposed a procedure based on the 3ω-SThM to measure the thermal exchange radius, which is usually estimated but not experimentally measured. Not only this parameter limits the lateral spatial resolution but also its precise estimation is crucial for an accurate identification of the thermal conductivity at nanometric scale.

We have measured the thermal exchange radius of two commercial probes: the classical well-known Wollaston probe and a new Pd/SiO_2 probe. We have shown that the measured value for the Wollaston probe is quite different from previously estimated values. In addition, the Pd/SiO_2 probe reveals very promising as it simultaneously gives topographic and thermal images with a far better spatial resolution (better than 100 nm) due to its smaller thermal exchange radius and with a shorter acquisition time due to its higher cut-off frequency.

Next step will consist of identifying the thermal conductivity of individual nanowires. For that purpose, a thermal model of the probe is necessary and we are now working on it.

ACKNOWLEDGMENTS

This work has been supported by the ANR PNANO.

[1] S. Sade, L. Nagli, and A. Katzir, Appl. Phys. Lett. **87**, 101109 (2005).
[2] J. Christofferson and A. Shakouri, Microelectron. J. **35**, 791 (2004).
[3] A. Rosencwaig, J. Opsal, W. L. Smith, and D. L. Wilenborg, Appl. Phys. Lett. **46**, 1013 (1985).
[4] J. Christofferson and A. Shakouri, Rev. Sci. Instrum. **76**, 024903 (2005).
[5] S. Grauby, S. Dilhaire, S. Jorez, and W. Claeys, Rev. Sci. Instrum. **74**, 645 (2003).
[6] S. Dilhaire, S. Grauby, S. Jorez, L.-D. Patino Lopez, J.-M. Rampnoux, and W. Claeys, Appl. Opt. **41**, 4996 (2002).
[7] C. C. Williams and H. K. Wickramasinghe, Appl. Phys. Lett. **49**, 1587 (1986).
[8] A. Majumdar, J. P. Carrejo, and J. Lai, Appl. Phys. Lett. **62**, 2501 (1993).
[9] A. Majumdar, J. Lai, M. Chandrachood, O. Nakabeppu, Y. Wu, and Z. Shi, Rev. Sci. Instrum. **66**, 3584 (1995).
[10] L. Shi, S. Plyasunov, A. Bachtold, P. L. McEuen, and A. Majumdar, Appl. Phys. Lett. **77**, 4295 (2000).
[11] L. Shi, J. Zhou, P. Kim, A. Bachtold, A. Majumdar, and P. L. McEuen, J. Appl. Phys. **105**, 104306 (2009).
[12] M. Nonnenmacher and H. K. Wickramasinghe, Appl. Phys. Lett. **61**, 168 (1992).
[13] S. Lefèvre, S. Volz, J.-B. Saulnier, C. Fuentes, and N. Trannoy, Rev. Sci. Instrum. **74**, 2418 (2003).
[14] M. Hinz, O. Marti, B. Gotsmann, M. A. Lantz, and U. Dürig, Appl. Phys. Lett. **92**, 043122 (2008).
[15] S. Grauby, A. Salhi, L.-D. Patino Lopez, W. Claeys, B. Charlot, and S. Dilhaire, Microelectron. Reliab. **48**, 204 (2008).
[16] Y. Zhang, C. L. Hapenciuc, E. E. Castillo, T. Borca-Tasciuc, R. J. Mehta, C. Karthik, and G. Ramanath, Appl. Phys. Lett. **96**, 062107 (2010).
[17] S. Lefèvre and S. Volz, Rev. Sci. Instrum. **76**, 033701 (2005).
[18] K. J. Negus, M. M. Yovanovich, and J. V. Beck, ASME J. Heat Transfer **111**, 804 (1989).
[19] R. Prasher, Nano Lett. **5**, 2155 (2005).
[20] Y. Ezzahri, L. D. Patino Lopez, O. Chapuis, S. Dilhaire, S. Grauby, W. Claeys, and S. Volz, Superlattices Microstruct. **38**, 69 (2005).
[21] A. Majumdar, Annu. Rev. Mater. Sci. **29**, 505 (1999).
[22] S. Lefèvre, J.-B. Saulnier, C. Fuentes, and S. Volz, Superlattices Microstruct. **35**, 283 (2004).
[23] J. Westwater, D. P. Gosain, S. Tomiya, S. Usui, and H. Ruda, J. Vac. Sci. Technol. B **15**, 554 (1997).